Stiffness-matched biomaterial implants for cell delivery: clinical, intraoperative ultrasound elastography provides a 'target' stiffness for hydrogel synthesis in spinal cord injury

Jon Prager[1,2] (ID), Christopher F Adams[3], Alexander M Delaney[3], Guillaume Chanoit[1], John F Tarlton[1], Liang-Fong Wong[4], Divya M Chari[3] and Nicolas Granger[2] (ID)

Abstract

Safe hydrogel delivery requires stiffness-matching with host tissues to avoid iatrogenic damage and reduce inflammatory reactions. Hydrogel-encapsulated cell delivery is a promising combinatorial approach to spinal cord injury therapy, but a lack of *in vivo* clinical spinal cord injury stiffness measurements is a barrier to their use in clinics. We demonstrate that ultrasound elastography – a non-invasive, clinically established tool – can be used to measure spinal cord stiffness intraoperatively in canines with spontaneous spinal cord injury. In line with recent experimental reports, our data show that injured spinal cord has lower stiffness than uninjured cord. We show that the stiffness of hydrogels encapsulating a clinically relevant transplant population (olfactory ensheathing cells) can also be measured by ultrasound elastography, enabling synthesis of hydrogels with comparable stiffness to canine spinal cord injury. We therefore demonstrate proof-of-principle of a novel approach to stiffness-matching hydrogel-olfactory ensheathing cell implants to 'real-life' spinal cord injury values; an approach applicable to multiple biomaterial implants for regenerative therapies.

Keywords

Spinal cord injury, stiffness matched hydrogel biomaterials, spinal cord elasticity, olfactory ensheathing cell transplant, ultrasound elastography

Date received: 11 April 2020; accepted: 21 May 2020

Introduction

Biocompatibility and tissue-matching of implanted biomaterials is a major consideration in tissue engineering, particularly when translation from the lab to the clinic is the primary aim. An important component of biocompatibility is stiffness, which is of particular concern in the central nervous system (CNS) due to its relatively soft nature.[1] Increased inflammatory and immunological responses have been reported after implant of stiff materials in the CNS, for example, in a direct comparison of soft (100 Pa) compared to stiff (30 kPa) polyacrylamide gel implantation into rat brain,[2] and after electrode implant on the spinal cord.[3] Reduced host inflammatory cell numbers are seen in rodent studies where hydrogels of similar stiffness to spinal cord injury (SCI) are transplanted.[4,5]

Hydrogel implantation offers multiple benefits for SCI therapy. Hydrogels form a substitute extracellular matrix and porous structure which modifies the injury environment promoting cellular and axon infiltration.[6,7] Hydrogels can be used as a vehicle for molecular,[8] drug[9] or cell-based[10,11] 'combinatorial' therapies (for reviews see[12–15]). These can

[1]Bristol Veterinary School, University of Bristol, Bristol, UK
[2]The Royal Veterinary College, University of London, Hatfield, UK
[3]Cellular and Neural Engineering Group, Institute for Science and Technology in Medicine, Keele University, Keele, UK
[4]Bristol Medical School, University of Bristol, Bristol, UK

Corresponding author:
Nicolas Granger, The Royal Veterinary College, University of London, Hatfield AL9 7TA, UK.
Email: nicolasgranger@rvc.ac.uk

have synergistic effects, for example, lack of cell survival and integration is one of the main barriers to developing a clinically effective cell-based treatment for SCI.[16] Encapsulation of cells within a hydrogel has been demonstrated to increase cell survival after CNS transplant in rodent models.[10,17,18] Injectable materials can mould to the injury lesion before polymerisation *in situ*[15] allowing minimally invasive delivery. The adaptation of minimally immunogenic and previously US Food and Drug Administration (FDA)-approved materials for encapsulated cell delivery could further accelerate clinical hydrogel use.[19]

Despite these valuable benefits and advances, a robust approach to stiffness matching of hydrogels to the spinal cord on clinics has not been developed. Indeed, there is limited information available for spinal cord applications, particularly *in vivo* stiffness values; the stiffness of *in vivo* injured spinal cord is unknown. This knowledge gap represents a major obstacle to safe implantation of hydrogels on clinics. The majority of previous studies on spinal cord stiffness have been conducted *ex vivo* and post-mortem, and existing *in vivo* studies have used mechanical tensile measures[20–23] which require manipulation and dissection of the cord that would clearly be inappropriate for clinical patients. This precludes matching of a hydrogel implant to a patient's specific injury, required for development of personalised therapies.

We therefore aimed to establish a clinical method to determine the stiffness of injured spinal cord, and to use this as a tool to match hydrogel stiffness. Ultrasound elastography (USE) is a non-invasive method of determining the stiffness of a tissue. It has been successfully used in people for ancillary diagnosis of mammary neoplasia[24] and staging of liver fibrosis,[25] and has been applied to the spinal cord of experimental dogs where large areas of the spinal cord were exposed.[26] Acoustic radiation force impulse USE detects the speed of displacement of target tissue (shear wave velocity) in response to an acoustic impulse generated from the ultrasound transducer. This speed varies with the stiffness of the tissue[27] and can be mathematically converted to modulus of elasticity[28,29] allowing quantitative comparisons; materials with a higher elastic modulus will be stiffer and deform less for a given stress. The technique is relatively straightforward to perform, and we hypothesised could provide a readily clinically available method to obtain measures of the stiffness of spinal cord in the clinic.

To test this hypothesis, we used the clinical canine translational model of SCI,[30–32] companion dogs with spontaneous SCI presenting to referral veterinary hospitals. These animals represent a well-established large animal model of SCI[30–33] with heterogeneous and mixed compressive-contusive lesions similar to those seen in humans.[34] The model provides an important means of screening experimental interventions for feasibility and efficacy in a clinical setting.[33,35] Testing intraoperative spinal cord USE within a referral veterinary hospital presents similar challenges and logistical constraints to those faced

in a human hospital in terms of available time and access, safety, sterility, and operation of ultrasound equipment.

Having obtained USE data for *in vivo* injured and normal spinal cord, we applied the same USE technique to collagen hydrogels to investigate matching of a biomaterial implant to clinically determined SCI stiffness. Collagen hydrogels were tested with or without encapsulation of canine olfactory ensheathing cells (OECs). OECs represent an important, clinically relevant cell transplant population for SCI. They have been shown to improve walking (BBB score) in two recent meta-analyses of rodent experiments,[36,37] have shown efficacy in a clinical trial using the canine model[33] and have undergone phase 1 human trials demonstrating safety.[38] OECs have high viability encapsulated in collagen,[39] supporting the use of collagen as a protective delivery vehicle for OEC transplant.

Our aims were therefore to (1) test the feasibility of intraoperative spinal cord USE during therapeutic surgery, (2) generate stiffness measures for large animal natural SCI providing a 'target' stiffness for hydrogel synthesis, and (3) establish comparative USE measures of collagen hydrogel stiffness with encapsulation of a clinically relevant cell population (OECs).

Methods

Canine OEC culture

Canine mucosal OECs used in these experiments were obtained from cells preserved during a previous canine clinical trial,[33] and cultured as previously described.[33,40,41] Briefly, cells were cultured on poly-L-lysine (Sigma) coated flasks in media consisting of low glucose Dulbecco's Modified Eagle's Media (Sigma), 10% foetal bovine serum (Gibco), and 1% penicillin and streptomycin (Sigma) with added growth factors: 20 ng/mL neuregulin-1 (R&D Systems) and 2 μM forskolin (Sigma). Media was replaced every 3–4 days until cell confluence was observed then passaged into further flasks or split according to cell count by haemocytometer for encapsulation in collagen hydrogel as detailed below. Purified OEC cultures were obtained using the differential attachment strengths of OECs and fibroblasts as previously reported.[33,42]

Collagen hydrogel synthesis and OEC encapsulation

Collagen hydrogels were synthesised as previously described.[43] Briefly, type 1 rat tail collagen (Corning High Concentration, Scientific Laboratory Supplies Ltd), was diluted in 0.02M acetic acid to a range of concentrations; 4.5, 6.0, 7.5 mg/mL. 10x minimum essential media α (Gibco, with nucleosides) was added followed by neutralisation with 1M sodium hydroxide. All reagents were kept on ice. After neutralisation, 500 μL of hydrogel was transferred to 48-well plates and incubated for 20 min at 37°C in 5% CO_2.

Encapsulation of OECs was achieved by directly resuspending a cell pellet (obtained after centrifuging cells in solution at 1000 r/min for 5 min) with the neutralised liquid collagen mixture prior to incubation as above. OECs were encapsulated at a concentration of 1.25 million cells per 100 μL hydrogel (equivalent to previous canine transplants[33]). Once gelled after 20-min incubation, hydrogels were removed from the 48-well plates, submerged in cell culture medium (as defined above) in 24-well plates and maintained at 37°C in 5% CO_2.

Immunocytochemical procedures

Cells for immunocytochemistry were prepared on poly-L-lysine coated glass coverslips and fixed with 4% paraformaldehyde for 10 min at room temperature. Fixed cells were washed with 0.3% Triton in phosphate buffered saline (PBS), blocked for 1 h in 10% normal goat serum (Vector Laboratories) then incubated with primary antibody overnight at 4°C: mouse anti-nerve growth factor receptor (p75) (MAB5364, Millipore) at 1:200 to label OECs and rabbit anti-fibronectin (AO245, DAKO) at 1:400 to stain for fibroblast contaminants in the primary OEC cultures. Complementary secondary antibodies (anti-mouse 546 (Abcam) and anti-rabbit 660 (Abcam)) were applied at 1:500 dilution for 2 h at room temperature and coverslips mounted using hard-set mounting media with 4′,6-diamidino-2-phenylindole (DAPI) (Vectashield). To characterise the cultured OEC population, cell counts per 10x field were performed (n=5). Total cell number per field was determined by DAPI nuclear staining and the percentage of p75 and fibronectin positive cells determined by counting on Fiji ImageJ.[44]

LIVE/DEAD staining was performed by washing cell-hydrogel construct with 37°C PBS followed by immersion for 1 h in 4μM calcein and 6μM ethidium homodimer at 37°C. Confocal images were obtained immediately after staining using a Leica SP5-AOBS confocal laser scanning microscope attached to a Leica DM I6000 inverted epifluorescence microscope. For each gel, 3–4 image stacks through the depth of the gel were obtained from random areas and number of LIVE and DEAD stained cells quantified for each z-plane using a custom Fiji/ImageJ macro running thresholding and segmentation followed by particle analysis. The number of LIVE cells out of total LIVE and DEAD stained cells was expressed as a percentage (% LIVE) and averaged for each image stack and gel.

Mechanical indentation measurement of elasticity

To allow direct comparison of standard mechanical indentation and USE measurements, both measures were performed on Zerdine™ hydrogel samples of manufacturer certified stiffness. Zerdine™ is a proprietary polymer hydrogel based on polyacrylamide.[45] Indentation testing was conducted using a Universal Testing Machine 3367 (Instron) fitted with a 10 N load cell and 2 mm radius cylindrical indenter. Cylindrical Zerdine™ samples (radius 3.4 mm and height 8 mm) were deformed at a rate of 0.02 mm/s up to a maximum of 5 mm or 3 N of force. The best-fit line forming the gradient of the linear section of the resulting force-extension graph (0–10% strain) was used to obtain a value for stiffness in N/mm. This was converted to Young's modulus (Pa) using published methods[46] assuming that gels behave as a thin elastic layer on a rigid surface.[43,47,48] Briefly, published finite element analysis defines the load–depth relationship for a given ratio of indenter radius:layer thickness, which can then be substituted into

$$P = \frac{2E}{1-v^2}\, ah\left(FEA\right)$$

where P = load, E = Young's modulus, v = Poisson's ratio, a = radius of indenter, h = indentation depth/extension, FEA = finite element analysis constant. By rearranging for E and substituting the described N/mm gradient for the term 'P/h', Young's modulus can be calculated. The value for 'FEA' is based on gel and indenter size and in our set-up = 1.48.

USE

All USE was performed using a Siemens Acuson S2000 (Siemens Healthcare, Erlangen, Germany) with 'Virtual Touch Imaging Quantification' Acoustic Radiation Force Impulse imaging software using a 9 L4 linear matrix array transducer operating at 8 MHz. The region of interest size with this probe was 5 mm x 5 mm. An error, depicted as 'x.xx' m/s, is returned if the confidence level between tracking beams is below 80%.[49] If 'x.xx m/s' was returned, the measurement was discounted and repeated.

Recorded shear wave velocities (m/s) were converted to Young's modulus of elasticity (kPa) using previously published methods.[28,29] Briefly, shear wave velocity can be converted to shear modulus by $G = \rho c^2$ *(where G = shear modulus, ρ = density of material, and c = shear wave velocity)* and shear modulus can be converted to Young's modulus by $G = E\,/\,(2(1+v))$ *(where E = Young's modulus, v = Poisson's ratio)*. Young's modulus was therefore calculated by $E = (2(1+v))\,\rho c^2$. Poisson's ratio and density are material dependent, and values used are reported in the relevant sections below. Calculated values reported as modulus of elasticity are therefore taken to be the Young's modulus.

Calibration of USE. An elastography phantom (Elasticity QA Phantom model 049A, Computerised Imaging Reference Systems, Norfolk, VA) was used to allow calibration of our USE measures. The phantom contains four stepped

diameter cylindrical Zerdine™ 'targets' of known stiffness (10, 14, 46 and 86 kPa) in background (27 kPa). Stiffnesses are certified by manufacturer's mechanical testing. Ten measurements were taken from each of the four cylinders at a consistent point along their length (section of diameter 16.7 mm, comparable to spinal cord). Measurements from background were taken at a consistent depth of 3 cm. The manufacturer reports Zerdine™ to have a density of 1.04 ± 0.01 g/cm^3 and a Poisson's ratio of 0.5.[50]

USE of Zerdine. As described above, additional samples of Zerdine™ hydrogel at varying certified elasticities were used to provide a direct comparison between USE and mechanical indentation measures. For USE measures Zerdine cylinders 12 mm diameter and 10 mm long were submerged to a depth of 2 cm in PBS and 20 measures obtained from the centre of each sample.

USE of canine cadaver spinal cord. As initial proof-of-principle that USE could be used on canine spinal cord, measurements were performed on canine cadaveric specimens from clinical cases undergoing *post-mortem* examination at Bristol Veterinary School, having been euthanized at owners' request for medical reasons unrelated to this study and for conditions not involving the spinal cord. Written owner consent was obtained and ethical approval gained from the University of Bristol local ethical review panel (VIN/16/004). Dogs were excluded if they had spinal cord pathology determined based on clinical signs or gross post-mortem examination.

The spinal cord was removed from the vertebral column within 6 h of euthanasia and placed in isotonic saline solution. The spinal cord was transversely sectioned to obtain the C1-T2, T3-L3 and L4-S4 spinal segments which were immobilised in plastic containers. The ultrasound transducer was positioned in contact with the saline and the cord viewed in sagittal section at a depth of 2 cm. The hyperechoic central canal was visualised along the length of the ultrasound window to ensure the probe was held parallel and repeat measurements (n = 5) of shear wave velocity were taken from 5 regions (cervical, cervical intumescence, thoracic, lumbar, lumbar intumescence) of each cadaver cord.

USE of intraoperative canine spinal cord. Dogs, 5–20 kg, undergoing spinal cord decompressive surgery following acute thoracolumbar intervertebral disc extrusion were recruited at Langford Vets (Bristol Veterinary School Small Animal Hospital). These dogs present with signs of transverse myelopathy such as back pain, pelvic limb ataxia, paresis, paralysis, incontinence and loss of pain sensation in the worst cases. Ethical approval (VIN/15/036) and informed verbal owner consent was obtained.

Anaesthesia was at the discretion of the attending veterinary anaesthetist; consisting of pre-medication, intravenous induction, tracheal intubation and maintenance on inhalational anaesthetic in oxygen, with appropriate clinical monitoring and analgesia throughout surgery and recovery. The spinal cord was exposed by hemilaminectomy or mini-hemilaminectomy and the compressive disc material removed. The ultrasound probe was placed in contact with sterile saline at 37°C filling the surgical site as previously reported.[51] Sterility was maintained by placing the ultrasound transducer in either a sterile glove or sterile sleeve (Safersonic Medizinprodukte, Austria) based on surgeon preference, with the cable in a sterile endoscope sleeve passed to an operator at the ultrasound machine. The spinal cord was initially visualised in B-mode ultrasound for orientation in a sagittal plane, with orientation being confirmed by visualisation of the hyperechoic central canal between the hyperechoic dura. The region of interest box was positioned over the spinal cord at the lesion site ('lesion epicentre') and as far cranial and caudal to it as possible within the surgical window (approximately 1–2 cm). Cranial and caudal measures of shear wave velocity were combined in one data set ('lesion periphery'). Three repeat measures were recorded at each location (lesion epicentre, cranial and caudal) where the cord could be reliably visualised.

Poisson's ratio can be assumed to be 0.5 for soft tissue.[29] The density of canine spinal cord is unknown but human spinal cord has been reported[52] as 1.03 g/cm^3, so this value was used for calculations as an approximation.

USE of hydrogels and hydrogel encapsulating OECs. Collagen hydrogels $\pm$ OECs, synthesised as above ($n = 3–4$ per concentration) were measured by USE within 2 h of cell encapsulation (day 0) then at 24 and 72 h. For measurement, gels were moved with a spatula onto sterile 10% gelatin submerged in sterile 37°C PBS. Twenty measurements were recorded from the centre of each gel at a depth of 2 cm at each time point before being moved back to fresh cell culture medium in 24-well plates. Measurements of shear wave velocity were converted to Young's modulus as described above based on a Poisson's ratio of 0.5 and density[48] of 1 g/cm^2.

Statistical analysis

Data were tested for normality using the Shapiro-Wilk test. Parametric data were analysed using means, t-test, linear regression and analyses of variance (ANOVAs) with post hoc Tukey tests. Unless otherwise stated error bars are standard deviation and statistical significance is displayed as $* = p < 0.05$, $** = p < 0.01$, $*** = p < 0.001$. Non-parametric data were assessed with median, range, inter-quartile range, Mann–Whitney U, Kruskall-Wallis and Dunn's post hoc tests. All statistical analysis was performed in either Graphpad Prism (v8.3.0, GraphPad Software, La Jolla California USA) or RStudio (v 1.1.463).[53]
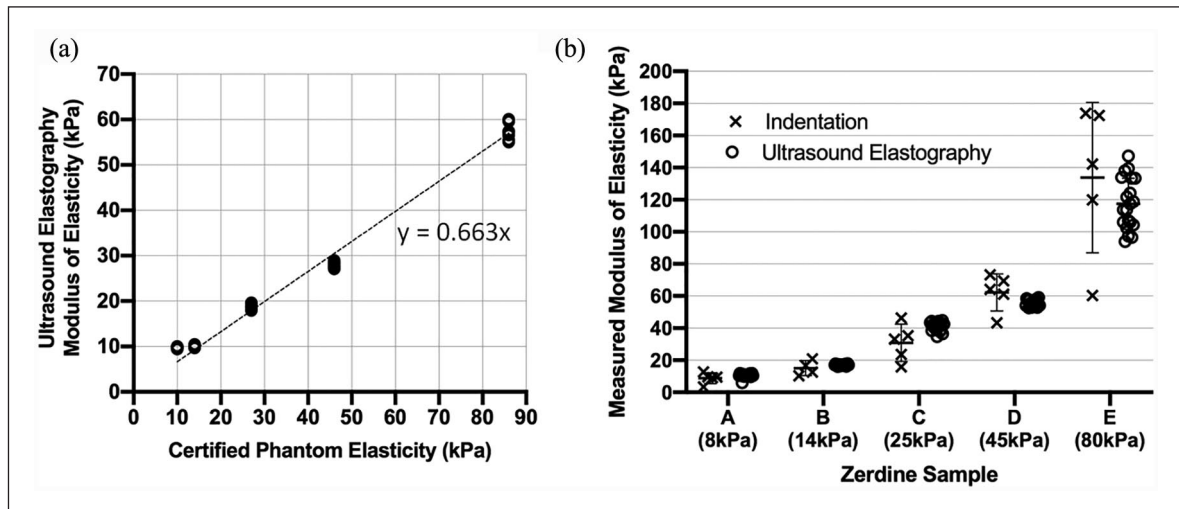
Figure 1. Calibration and validation of ultrasound elastography. (a) Ultrasound elastography stiffness measures ($n=10$) of certified ultrasound elasticity phantom values (stiffnesses: 10, 14, 27, 46, 86 kPa) are shown along with the line of linear regression. All further presented values for ultrasound elastography are calibrated using this conversion. (b) A comparison between ultrasound elastography and standard mechanical indentation measurements of elasticity was made on five different Zerdine™ hydrogel samples to validate ultrasound elastography measures. No significant difference was seen between measurement techniques across the range of samples (8–80 kPa; two-way ANOVA).

Results

USE calibration and validation

A strong, positive, linear correlation was seen between certified phantom elasticity values and USE measures ($r=0.996$, $R^2=0.991$, $p=0.0003$) (Figure 1(a)). The equation of the line of linear regression ($y=0.663x$, where 'y' is measured elastic modulus and 'x' is phantom elastic modulus) defines this relationship and allows calibration of the ultrasound measures in our set-up. All subsequent USE measures reported here are corrected by this calibration.

A comparison between USE and mechanical indentation elasticity measures of five samples of Zerdine™ (Figure 1(b)) across a range of elasticities from 8 to 80 kPa shows no significant difference between the two techniques (two-way ANOVA).
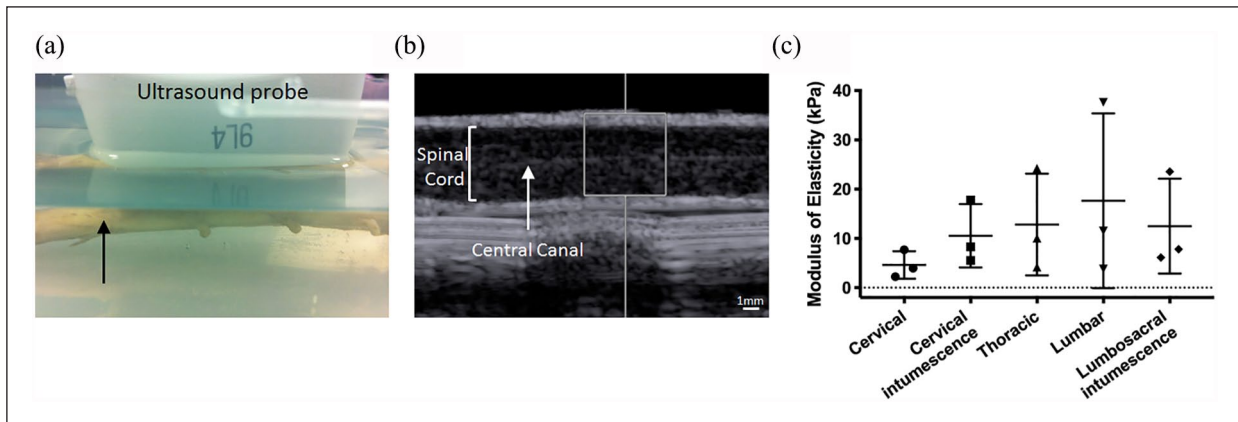
USE measures of spinal cord

USE of cadaver canine spinal cord demonstrates applicability of the technique to spinal cord. Three dogs were used for investigation of cadaver cord. Their ages ranged from 5 to 7 years; breeds included a Sprocker, Bull Mastiff cross and Flat Coat Retriever. Causes of death were haemolytic anaemia, left cerebral hemisphere glioma, and dilated cardiomyopathy respectively.

Ultrasound images of the spinal cord were clear when scanning submerged in saline (Figure 2(a) and (b)). No significant difference was seen between regions of cadaver spinal cord (one-way ANOVA) (Figure 2(c)) and an overall average cadaver spinal cord modulus of elasticity was calculated as 11.6 ± 4.7 kPa.

Clinical intraoperative USE of canine spinal cord is feasible. Fifteen dogs with injury between T3 and L3 spinal cord segments were recruited. The transducer could be simply oriented towards the spinal cord in contact with saline filling the surgical approach to visualise the spinal cord (Figure 3(a)). In 2 dogs, the spinal cord could not be reliably visualised through a smaller mini-hemilaminectomy approach. For the remaining 13 animals: 4 had mini-hemilaminectomies and 9 had hemilaminectomies; ages ranged from 4 to 8 years; 9 animals were male and 4 female; breeds included six Dachshunds, two Cocker Spaniels, one Beagle, Basset Hound, Labrador, Jack Russel Terrier and Cavalier King Charles Spaniel cross Pug. All animals were in the acute or sub-acute phase of injury,[54] at less than 2 weeks from first onset of clinical signs, with the majority in the acute phase. They showed clinical signs ranging from paraparesis (n=9) to paraplegia with loss of pain sensation in the pelvic limbs (n=4).

After visualisation of the spinal cord (Figure 3(b)), areas of compression could be readily identified by: (1) visualisation of hyperechoic disc material ventral to the spinal cord, (2) loss of visible hyperechoic central canal within spinal cord, (3) narrowing and/or irregularity of hyperechoic dura mater dorsal and/or ventral to the spinal cord, and (4) direct surgeon visualisation. Intraoperative USE was feasible, and measures of shear wave velocity could be obtained from the spinal cord. In three animal readings could not be obtained for all locations (lesion epicentre, cranial and caudal at the lesion periphery).

Variability of intraoperative USE measures was assessed by determining the coefficient of variation for peripheral and lesion epicentre measures for each dog (Figure 3(c)). The average coefficient of variation for

Figure 2. Ultrasound elastography stiffness measures of cadaver spinal cord. *Ex vivo* spinal cord samples from fresh canine cadavers were suspended in saline and the ultrasound probe held 3 cm away in contact with the saline to image in sagittal section (a, black arrow is spinal cord). The spinal cord was clearly visible on the resulting ultrasound images, with the hyperechoic central canal identifiable (b, white square shows 5 mm x 5 mm region of interest for stiffness measurements). Ultrasound elastography measurements at 5 points along the length of the dissected spinal cord in 3 dogs (c) show no significant difference between regions (one-way ANOVA).

peripheral and lesion epicentre spinal cord was similar at $32.0\% \pm 12.1\%$ and $31.0\% \pm 22.6\%$ respectively. The median distance from transducer to spinal cord (i.e. measurement depth) was 19.5 mm, with a range of 16–25 mm. No significant correlation was seen between depth and either peripheral or lesion epicentre stiffness measures across this relatively small range.

Stiffness of lesion epicentre is significantly lower than periphery spinal cord. Intraoperative USE measures of the spinal cord at the lesion epicentre had a significantly lower modulus of elasticity than at the lesion periphery ($p = 0.0056$, Mann–Whitney U), with a median of 18.3 kPa (inter-quartile range (IQR): 11.6–31.1 kPa) and 47.9 kPa (IQR: 32.6–81.7 kPa) respectively (Figure 3(d)). It was noted that the only 2 dogs in this cohort whose modulus of elasticity was not lower at the lesion compared to peripheral spinal cord were the only dogs in this cohort who did not recover sensation and motor function after injury (grey arrows mark these 2 cases in Figure 3(d)).

Comparison of intraoperative measures to earlier cadaver measures shows a significant difference between cadaver and intraoperative peripheral spinal cord stiffness ($p = 0.0254$, Kruskall Wallis followed by Dunn's multiple comparison test). There is no significant difference between cadaver and intraoperative lesion epicentre measures.

## Encapsulation of canine OECs in high concentration collagen hydrogel

USE of large, high collagen concentration hydrogels is feasible. Collagen hydrogels of diameter 11 mm (Figure 4(a)) could be reliably imaged by ultrasound when submerged in saline (Figure 4(b)). Measurements of stiffness by USE

(Figure 4(c)) show a strong linear correlation between increasing collagen concentration and increasing stiffness ($r = 1.0$, $R^2 = 1.0$, $p < 0.0042$; equation of line of linear regression y = 1.57x − 4.36).

OEC viability is not significantly affected by collagen concentration. Canine OEC culture populations were characterised by immunofluorescence cytochemistry before encapsulation, with no contaminant fibroblasts seen (Figure 5(a)). Culture of OECs within large, high collagen concentration hydrogels was possible with normal bipolar, spindle shaped OEC morphology seen through the depth of hydrogel by immunofluorescence (Figure 5(b)). LIVE/DEAD staining (Figure 5(c)) showed no significant difference (two-way ANOVA) in proportion of live cells between collagen concentrations (4.5–7.5 mg/ml). There was an overall significant effect of time ($F(1, 15) = 10.2$, $p = 0.006$; two-way ANOVA) but no significant difference within any collagen concentration in the proportion of live cells between day 1 and 3 (post hoc Tukey test). The overall average proportion of live cells was $91.1\% \pm 1.9\%$ on day 1 and $76.3\% \pm 7.3\%$ on day 3 (Figure 5(d)).

Encapsulation of OECs increases collagen hydrogel stiffness. Within 2 h after encapsulation of OECs, the stiffness of all hydrogel constructs was increased compared to acellular hydrogels (fold increase in mean: 1.25 in 4.5 mg/ml, 1.57 in 6 mg/ml, 1.73 in 7.5 mg/ml) (Figure 6(a)). This increase was significant in the 6 mg/ml and 7.5 mg/ml gels ($F(1, 12) = 57$, $p < 0.0001$ for encapsulation on two-way ANOVA, post hoc Tukey test $p = 0.012$ and $p < 0.0001$ respectively).

Stiffness of these cellular hydrogel constructs is also significantly increased with increasing collagen concentration ($F(2, 12) = 106$, $p < 0.0001$ for collagen concentration
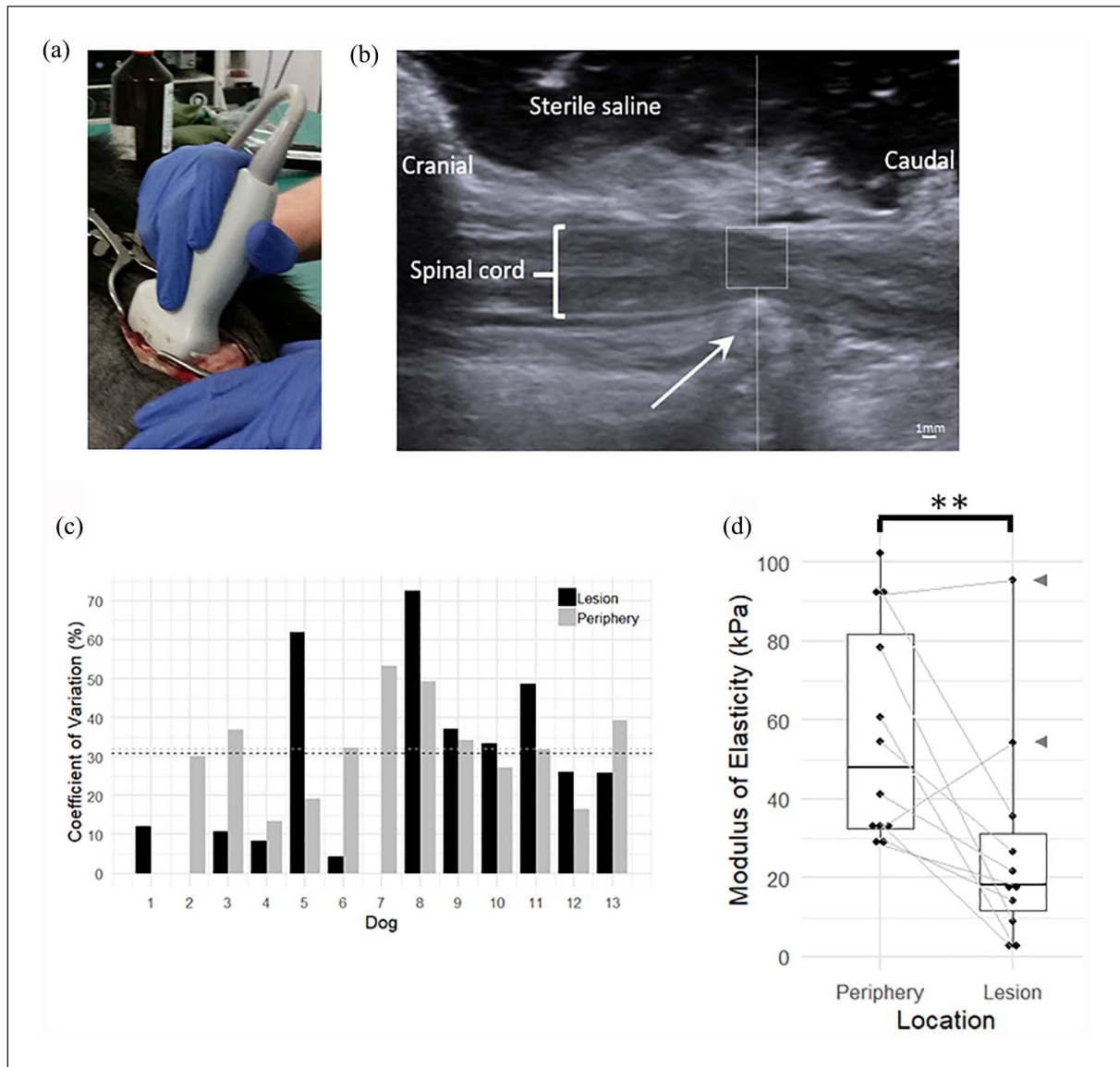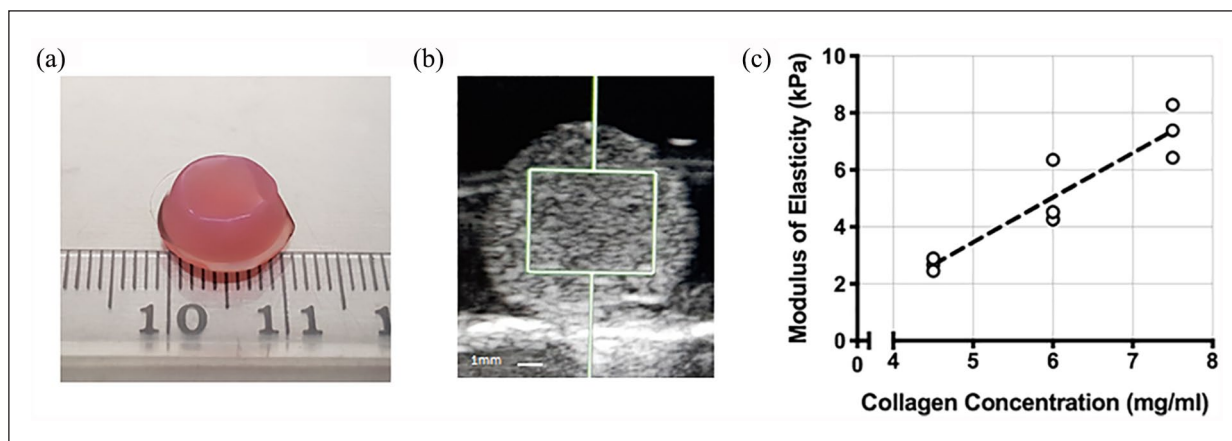
Figure 3. Ultrasound elastography stiffness measures of *in vivo* intraoperative spinal cord. Intraoperative ultrasound elastography stiffness measures were performed by placing the ultrasound transducer within the surgical incision filled with saline (a, non-surgical/non-sterile example of set-up). An example *in vivo* intraoperative ultrasound image of the spinal cord is shown in (b). The injury site can be identified with herniated disc visible (white arrow) and loss of hyperechoic central canal due to compression of the cord at this site. The coefficient of variation for lesion epicentre (black) and lesion periphery (grey) measures are graphed for each dog (c). Horizontal dotted lines show average coefficient of variation for lesion epicentre (black, 31.0%) and lesion periphery (grey, 32.0%). Missing columns reflect measures unable to be obtained. A significantly decreased modulus of elasticity ($p=0.0056$, Mann-Whiney U, $n=13$) is seen at the lesion compared to peripheral cord intraoperatively (d). Dots mark average measured values for each dog, grey lines denote comparison within same dog where this is possible ($n=10$), grey arrows mark the only 2 dogs where modulus of elasticity is not lower at the lesion.

on two-way ANOVA) with a linear correlation ($r=0.99$, $R^2=0.98$, $p=0.0060$; equation of line of linear regression $y=3.14x-10.8$).

Over 3 days of culture, there is a significant effect of time on hydrogel construct stiffness when measured by USE ($F(2, 24)=12$, $p=0.0002$ repeated measures two-way ANOVA) (Figure 6(b)). The highest concentration 7.5 mg/ml collagen hydrogel encapsulating OECs significantly increases stiffness in the first 24 h of culture ($p=0.0087$, post hoc Tukey test) and further increases stiffness to day 3 ($p=0.016$ compared to day 1, $p<0.0001$ compared to day 0). Other cellular collagen concentrations and acellular hydrogels do not change stiffness when kept in cell culture conditions (37°C, 5% CO_2) for 3 days (no significant difference between days, post hoc Tukey test).
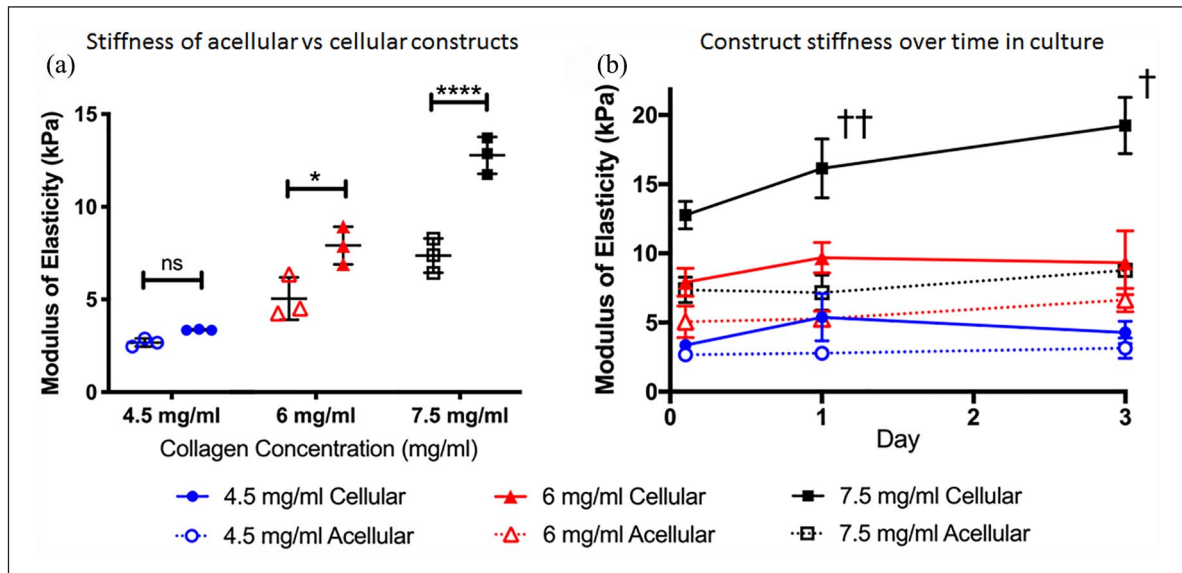
Figure 4. Ultrasound elastography stiffness measurement of collagen hydrogels. Large, cylindrical (11 mm diameter, 0.5 ml volume) collagen hydrogels were synthesised (a) and measured by ultrasound elastography submerged in saline (b). A linear correlation was seen between increasing collagen concentration and increasing modulus of elasticity (c) ($r = 1.0$, $R^2 = 1.0$, $p < 0.0042$).
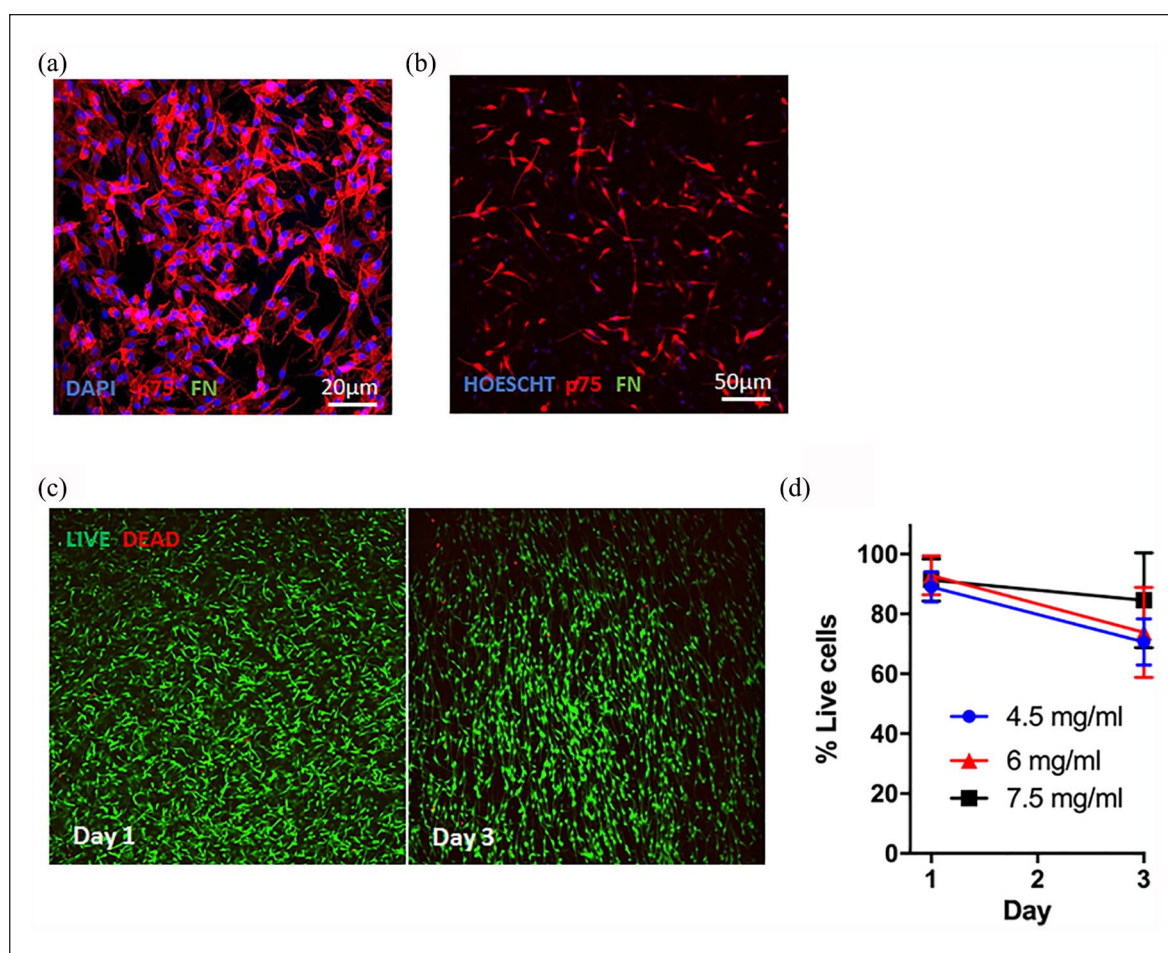
Figure 5. OEC viability in large, high collagen concentration hydrogels. An example immunofluorescence image of canine OECs immunostained for p75 (red, OECs) and fibronectin (green, FN, fibroblasts, none seen) is shown before (a) and after encapsulation in hydrogel (b). Example confocal images are shown of encapsulated OECs LIVE (green) and DEAD (red) stained within 7.5 mg/ml collagen hydrogel at day 1 and 3 of culture (c). The proportion of live cells was determined (d) with no significant difference seen between collagen concentrations or time points (two-way ANOVA).

Figure 6. Effect of olfactory ensheathing cell encapsulation on hydrogel stiffness. Stiffness of collagen hydrogels (4.5, 6 or 7.5 mg/ml) was determined by ultrasound elastography before (open symbols) and immediately after (filled symbols) encapsulation of OECs (a). Encapsulation increased stiffness, reaching significance in 6 mg/ml and 7.5 mg/ml gels (two-way ANOVA, post hoc Tukey test; *$p = 0.012$, ****$p < 0.0001$). Continued culture to 3 days and repeated stiffness measurement (b) showed no change in stiffness of acellular gels over time (dotted lines), and an increased stiffness in gels encapsulating OECs at 7.5 mg/ml only (repeated measures two-way ANOVA, post hoc Tukey test; ††$p = 0.0087$ between day 0 and 1, †$p = 0.016$ between day 1 and 3 and $p < 0.0001$ between day 0 and 3).

Discussion

We report proof-of-concept of a clinically applicable, non-invasive and USE based approach to stiffness-matching of implantable hydrogels for SCI repair. To our knowledge, this is the first report of such a stiffness-matching approach for biomaterial therapies in neurological injuries.

Both machine[55] and transducer[56] can affect USE measures, even within ARFI elastography. This highlights the necessity to standardise USE values against known measures to allow valid comparison between centres and machine set-ups. This is particularly vital in order to provide a useable reference measurement to the biomaterials community and those developing novel materials. The USE data presented here have therefore been calibrated to a commercially available elasticity phantom and certified elasticities of Zerdine™, a proprietary, polyacrylamide-based hydrogel commonly used in elastography quality assurance.[28] Mechanical indentation is commonly used for elasticity testing in biomaterials testing and the close correlation between our indentation and USE measures of Zerdine™ provide confidence in the accuracy and reliability of our data.

Median intraoperative USE values for lesion epicentre (18.3 kPa), periphery (47.9 kPa) and values for cadaver canine spinal cord (11.6 kPa) determined here are within the range of values previously reported in the literature for spinal cord. A value of 18.5 ± 7 kPa was reported for uninjured *in vivo* cervical cord when measured by USE in

experimental dogs, although these measures were not calibrated.[26] The elasticity of spinal cord in anaesthetised experimental puppies and cats[22,23] was reported as 265 kPa when measured using mechanical methods (tensile extension at loads of 5–10 g). As with our findings, this was higher than measures of canine cadaver spinal cord under the same conditions (11.9–16.8 kPa).[1,20] *Ex vivo* measures of spinal cord give an even broader range of values, from 1.3 kPa in rats[57] (measured by indentation, maximum load 25 μN) up to 1.4 MPa in humans[58] (with high-strain tensile measurement up to 20% strain).

Due to the viscoelastic nature of spinal cord, the method of elasticity measurement and the precise testing parameters (e.g. strain of tensile measures[59] or frequency of oscillatory rheology[60]) can affect the modulus of elasticity determined. Notably, higher strain increases the measured modulus of elasticity[61,62] but changes in strain rate have been reported not to have an effect[58] (for a review see Bartlett et al.,[63]). For example, bovine spinal cord white matter measured by tensile measurement was reported to have a modulus of elasticity of 1.05 MPa with a strain of 40% and 115 kPa with a strain of 5% in the same study.[64] Reported measurements of spinal cord elasticity therefore need to be taken in the context of measurement parameters.

Furthermore, reports of spinal cord elasticity are mainly from post-mortem tissue. Time post-mortem and degree of tissue degradation, storage conditions, temperature and hydration status are additional variables that can affect elasticity measurement and contribute to the wide range in

reported values.[65,66] Inclusion or exclusion of meninges in sample dissection is important; human cadaveric spinal cord has been reported to have an elastic modulus of 1.4 MPa with intact pia mater and 89 kPa with cut pia mater in the same study with high strain (20%) tensile measurement.[58]

There are therefore a variety of experimental factors that make exact quantitative comparison between different measurement techniques and different studies extremely challenging. This has prevented simple comparison between spinal cord and biomaterial stiffness and is a major barrier to clinical hydrogel development and translation of experimental hydrogel therapies. Crucially, our approach utilises the same USE technique to measure both spinal cord and hydrogel. It avoids the problems inherent in comparing different elasticity measurement techniques and provides a direct comparison between *in vivo* tissue and *in vitro* hydrogel that is unreported for spinal cord.

When measured by USE, collagen hydrogels in this study (4.5–7.5 mg/ml collagen) have stiffnesses of the same order of magnitude as canine intraoperative injured spinal cord. For clinical transplant, we anticipate implant stiffness would be matched to the lowest stiffness in host tissue to avoid iatrogenic damage and ensure safe transplantation. Matching hydrogel stiffness to an individual patient's specific injury stiffness would be possible given the clear linear correlation we see between collagen concentration and modulus of elasticity.

OECs encapsulated within these stiffnesses of collagen hydrogel show high viability up to 3 days in culture, at an OEC concentration applicable to clinical transplants.[33] Clinical transplantation would likely occur within this 3-day time-period, if not immediately after encapsulation (prior to gelation) if a percutaneous injectable approach were used. Previous work has also shown high OEC viability after hydrogel encapsulation in lower concentration collagen hydrogels,[39] Matrigel[67] and polylactic-*co*-glycolic acid (PLGA)[68] hydrogels, although not in alginate.[67] Collagen hydrogels were used in this study because of their prior use in experimental SCI repair,[12,69] including for cell encapsulation,[70,71] and because collagen is highly biocompatible;[1] a variety of collagen products from various sources have been FDA approved for use in the nervous system,[72] including as medical sealants for dural repair.[73]

We report an increase in overall stiffness of the hydrogel construct after OEC encapsulation, and so highlight an important consideration for stiffness-matching and hydrogel synthesis. There is considerable literature assessing the effect of hydrogel stiffness on cell fate,[74–77] but less information on the effect of cell encapsulation on construct stiffness. Fibroblast encapsulation in collagen hydrogels has been reported to increase stiffness,[78] further increasing with continued culture.[78,79] This increased stiffness could be due to extracellular matrix (ECM) deposition by the cells,[78] protein adsorption to the collagen,[80] or a direct bulk effect of the high density of cells. The increased stiffness

with OEC encapsulation we observed was less marked than that reported with fibroblasts,[78,79] which may be due to the different functions of the cell types encapsulated. Unlike OECs, one of the main roles of fibroblasts is to contract tissue.[81] These findings emphasise the importance of testing hydrogel-cell constructs with a cell population that is clinically relevant to its intended use.

The stiffness changes in cell-hydrogel construct reported here have all been performed *in vitro* up to the point of transplant. However, the changes occurring in construct stiffness *in vivo* over time as host degradative enzymes and inflammatory cells interact with biodegradable materials are largely unknown. The manner in which SCI stiffness itself changes over time is also poorly understood; intraoperative USE measures could be used to investigate this further. These remain important areas for further study in tissue engineering.

These are the first *in vivo* SCI stiffness measures after natural injury, however, they corroborate experimental findings in rats that injured spinal cord is less stiff than surrounding spinal cord (previously measured using a custom microindentation system[57] and atomic force microscopy[82]). There is a known interaction between stiffness of substrate and axon growth, with axons tending to grow better on lower stiffness substrates *in vitro*[83–85] (for reviews see[86,87]). It has therefore been suggested that the lower stiffness seen in injured spinal cord in experimental models may be mechanically more permissive for axon regeneration.[57] Establishing that injured spinal cord tissue is also less stiff after natural injury in a large animal clinical model is therefore an important extension of the experimental rodent work.

Improved understanding about changes to spinal cord stiffness after injury could also inform approaches to SCI repair.[82] It would be particularly valuable to investigate the degree of axonal regeneration *in vivo* in response to stiffness queues, for example, after implant of varying stiffness hydrogels into sites of SCI, to determine the most appropriate stiffness of implant to promote axon regeneration.

Our data also raise the important possibility that clinical severity and recovery may be related to SCI stiffness. A thorough investigation was beyond the scope of this study, but it is noteworthy that the two most severely affected animals (the only animals who did not recover walking by 3 weeks after injury) had the highest stiffness at the SCI lesion and relative to surrounding cord. Using intraoperative USE could therefore represent a tool to facilitate further understanding of the relationship between clinical severity of injury and spinal cord mechanical properties, with correlation to recovery.

Conclusion

We have developed a protocol to non-invasively measure the *in vivo* stiffness of spinal cord after injury in a clinical setting, allowing us to provide a previously undetermined 'target' value for clear specification and direction of

hydrogel synthesis. Our work addresses a knowledge gap in the development of hydrogels for clinical use. We predict our method could be directly used in veterinary medicine in the context of trials testing implantation of an OEC-hydrogel construct for SCI repair. Importantly, reports of intraoperative spinal cord ultrasound in humans[88,89] suggest these principles could be directly applied to human clinics.

The approach presented here is highly versatile and applicable to multiple hydrogel delivery systems for a wide range of applications (e.g. cell or drug/biomolecule hydrogel delivery in many target tissues). It provides the ability to rapidly and simply measure the stiffness of individual injuries on clinics and match this to previously determined hydrogel construct stiffness. This may in the future allow bespoke hydrogel implants to be created for each patient at the time of transplant for 'personalised cell therapy'.

Author contributions

J.P. contributed to experimental design, conducted *in vivo* data collection and all *in vitro* experiments, analysed and interpreted the data, wrote the original draft, and approved the final version. C.A. contributed to experimental design, hydrogel synthesis, interpreted the data, critically revised the manuscript and approved the final version. A.D. conducted *in vivo* data collection, critically revised the manuscript and approved the final version. G.C. contributed to experimental design, interpreted the data, critically revised the manuscript and approved the final version. J.T. contributed to mechanical elasticity data collection and analysis, critically revised the manuscript, and approved the final version. L.W. contributed to experimental design, cell culture, interpreted the data, critically revised the manuscript and approved the final version. D.C. contributed to experimental design, interpreted the data, critically revised the manuscript and approved the final version. N.G. conceptualised the project, contributed to experimental design, conducted *in vivo* data collection, interpreted the data, critically revised the manuscript and approved the final version.

Declaration of conflicting interests

The author(s) declared no potential conflicts of interest with respect to the research, authorship, and/or publication of this article.

Ethical approval

Ethical approval was obtained from the University of Bristol local ethical review panel; VIN/16/004 for post-mortem work and VIN/15/036 for intraoperative study.

Informed consent

Owners of all pet dogs included in this study provided informed consent for intraoperative ultrasound elastography verbally and post-mortem procedures as part of written consent forms.

ORCID iDs

Jon Prager https://orcid.org/0000-0003-0488-5478
Nicolas Granger https://orcid.org/0000-0002-3036-3908

Data availability

All data related to this manuscript will be made available on request.

References

1. Aurand E, Wagner J, Lanning C, et al. Building biocompatible hydrogels for tissue engineering of the brain and spinal cord. *J Funct Biomater* 2012; 3: 839–863.
2. Moshayedi P, Ng G, Kwok JCF, et al. The relationship between glial cell mechanosensitivity and foreign body reactions in the central nervous system. *Biomaterials* 2014; 35(13): 3919–3925.
3. Minev IR, Musienko P, Hirsch A, et al. Biomaterials. Electronic dura mater for long-term multimodal neural interfaces. *Science* 2015; 347: 159–163.
4. Bakshi A, Fisher O, Dagci T, et al. Mechanically engineered hydrogel scaffolds for axonal growth and angiogenesis after transplantation in spinal cord injury. *J Neurosurg Spine* 2004; 1(3): 322–329.
5. Khaing ZZ, Milman BD, Vanscoy JE, et al. High molecular weight hyaluronic acid limits astrocyte activation and scar formation after spinal cord injury. *J Neural Eng* 2011; 8(4): 046033.
6. Perale G, Rossi F, Sundstrom E, et al. Hydrogels in spinal cord injury repair strategies. *ACS Chem Neurosci* 2011; 2: 336–345.
7. Haggerty AE, Marlow MM and Oudega M. Extracellular matrix components as therapeutics for spinal cord injury. *Neurosci Lett* 2017; 652: 50–55.
8. Hyatt A, Wang D, Kwok J, et al. Controlled release of chondroitinase ABC from fibrin gel reduces the level of inhibitory glycosaminoglycan chains in lesioned spinal cord. *J Control Release* 2010; 147: 24–29.
9. Perale G, Rossi F, Santoro M, et al. Multiple drug delivery hydrogel system for spinal cord injury repair strategies. *J Control Release* 2012; 159: 271–280.
10. Führmann T, Tam RY, Ballarin B, et al. Injectable hydrogel promotes early survival of induced pluripotent stem cell-derived oligodendrocytes and attenuates longterm teratoma formation in a spinal cord injury model. *Biomaterials* 2016; 83: 23–36.
11. Papa S, Vismara I, Mariani A, et al. Mesenchymal stem cells encapsulated into biomimetic hydrogel scaffold gradually

release CCL2 chemokine in situ preserving cytoarchitecture and promoting functional recovery in spinal cord injury. *J Control Release* 2018; 278: 49–56.

12. Macaya DJ, Hayakawa K, Arai K, et al. Astrocyte infiltration into injectable collagen-based hydrogels containing FGF-2 to treat spinal cord injury. *Biomaterials* 2013; 34(14): 3591–3602.

13. Khaing ZZ, Thomas RC, Geissler SA, et al. Advanced biomaterials for repairing the nervous system: what can hydrogels do for the brain? *Mater Today* 2014; 17: 332–340.

14. Donaghue IE, Tam R, Sefton MV, et al. Cell and biomolecule delivery for tissue repair and regeneration in the central nervous system. *J Control Release* 2014; 190: 219–227.

15. Siebert JR, Eade AM and Osterhout DJ. Biomaterial approaches to enhancing neurorestoration after spinal cord injury: strategies for overcoming inherent biological obstacles. *Biomed Res Int* 2015; 2015: 752572.

16. Tam RY, Fuehrmann T, Mitrousis N, et al. Regenerative therapies for central nervous system diseases: a biomaterials approach. *Neuropsychopharmacology* 2014; 39(1): 169–188.

17. Zhong J, Chan A, Morad L, et al. Hydrogel matrix to support stem cell survival after brain transplantation in stroke. *Neurorehabil Neural Repair* 2010; 24(7): 636–644.

18. Ballios BG, Cooke MJ, Donaldson L, et al. A hyaluronan-based injectable hydrogel improves the survival and integration of stem cell progeny following transplantation. *Stem Cell Reports* 2015; 4: 1031–1045.

19. Finch L, Harris S, Solomou G, et al. Safe nanoengineering and incorporation of transplant populations in a neurosurgical grade biomaterial, DuraGen PlusTM, for protected cell therapy applications. *J Control Release* 2020; 321: 553–563.

20. Tunturi AR. Elasticity of the spinal cord, pia, and denticulate ligament in the dog. *J Neurosurg* 1978; 48(6): 975–979.

21. Chang GL, Hung TK, Bleyaert A, et al. Stress-strain measurement of the spinal cord of puppies and their neurological evaluation. *J Trauma* 1981; 21(9): 807–810.

22. Hung TK and Chang GL. Biomechanical and neurological response of the spinal cord of a puppy to uniaxial tension. *J Biomech Eng* 1981; 103(1): 43–47.

23. Chang GL, Hung TK and Feng WW. An in-vivo measurement and analysis of viscoelastic properties of the spinal cord of cats. *J Biomech Eng* 1988; 110(2): 115–122.

24. Li Q, Wang L, Wu H, et al. Controlled study of traditional ultrasound and ultrasound elastography on the diagnosis of breast masses. *Ultrasound Q* 2015; 31(4): 250–254.

25. Li C, Zhang C, Li J, et al. Diagnostic accuracy of real-time shear wave elastography for staging of liver fibrosis: a meta-analysis. *Med Sci Monit* 2016; 22: 1349–1359.

26. Al-Habib A, Albakr A, Al Towim A, et al. In vivo assessment of spinal cord elasticity using shear wave ultrasound in dogs. *J Neurosurg Spine* 2018; 29(4): 461–469.

27. Nightingale K, Soo MS, Nightingale R, et al. Acoustic radiation force impulse imaging: in vivo demonstration of clinical feasibility. *Ultrasound Med Biol* 2002; 28(2): 227–235.

28. Oudry J, Lynch T, Vappou J, et al. Comparison of four different techniques to evaluate the elastic properties of phantom in elastography: is there a gold standard? *Phys Med Biol* 2014; 59: 5775–5793.

29. Nightingale K, McAleavey S and Trahey G. Shear-wave generation using acoustic radiation force: in vivo and ex vivo results. *Ultrasound Med Biol* 2003; 29(12): 1715–1723.

30. Jeffery ND, Smith PM, Lakatos A, et al. Clinical canine spinal cord injury provides an opportunity to examine the issues in translating laboratory techniques into practical therapy. *Spinal Cord* 2006; 44(10): 584–593.

31. Levine JM, Levine GJ, Porter BF, et al. Naturally occurring disk herniation in dogs: an opportunity for pre-clinical spinal cord injury research. *J Neurotrauma* 2011; 28(4): 675–688.

32. Moore SA, Granger N, Olby NJ, et al. Targeting translational successes through CANSORT-SCI: using pet dogs to identify effective treatments for spinal cord injury. *J Neurotrauma* 2017; 34: 2007–2018.

33. Granger N, Blamires H, Franklin RJM, et al. Autologous olfactory mucosal cell transplants in clinical spinal cord injury: a randomized double-blinded trial in a canine translational model. *Brain* 2012; 135(Pt 11): 3227–3237.

34. Smith PM and Jeffery ND. Histological and ultrastructural analysis of white matter damage after naturally-occurring spinal cord injury. *Brain Pathol* 2006; 16(2): 99–109.

35. Hu HZ, Granger N, Pai SB, et al. Therapeutic efficacy of microtube-embedded chondroitinase ABC in a canine clinical model of spinal cord injury. *Brain* 2018; 141: 1017–1027.

36. Watzlawick R, Rind J, Sena ES, et al. Olfactory ensheathing cell transplantation in experimental spinal cord injury: effect size and reporting bias of 62 experimental treatments: a systematic review and meta-analysis. *PLOS Biol* 2016; 14: e1002468.

37. Nakhjavan-Shahraki B, Yousefifard M, Rahimi-Movaghar V, et al. Transplantation of olfactory ensheathing cells on functional recovery and neuropathic pain after spinal cord injury; systematic review and meta-analysis. *Sci Rep* 2018; 8: 325.

38. Li L, Adnan H, Xu B, et al. Effects of transplantation of olfactory ensheathing cells in chronic spinal cord injury: a systematic review and meta-analysis. *Eur Spine J* 2015; 24(5): 919–930.

39. Adams CF, Delaney AM, Carwardine DR, et al. Nanoparticle-based imaging of clinical transplant populations encapsulated in protective polymer matrices. *Macromol Biosci* 2019; 19(2): e1800389.

40. Ito D, Fujita N, Ibanez C, et al. Serum-free medium provides a clinically relevant method to increase olfactory ensheathing cell numbers in olfactory mucosa cell culture. *Cell Transplant* 2008; 16: 1021–1027.

41. Carwardine D, Wong L-F, Fawcett JW, et al. Canine olfactory ensheathing cells from the olfactory mucosa can be engineered to produce active chondroitinase ABC. *J Neurol Sci* 2016; 367: 311–318.

42. Nash HH, Borke RC and Anders JJ. New method of purification for establishing primary cultures of ensheathing cells from the adult olfactory bulb. *Glia* 2001; 34: 81–87.

43. Adams CF, Dickson AW, Kuiper J-H, et al. Nanoengineering neural stem cells on biomimetic substrates using magnetofection technology. *Nanoscale* 2016; 8: 17869–17880.

44. Schindelin J, Arganda-Carreras I, Frise E, et al. Fiji: an open-source platform for biological-image analysis. *Nat Methods* 2012; 9: 676–682.

45. Hungr N, Long J-A, Beix V, et al. A realistic deformable prostate phantom for multimodal imaging and needle-insertion procedures. *Med Phys* 2012; 39(4): 2031–2041.

46. Cao Y, Ma D and Raabe D. The use of flat punch indentation to determine the viscoelastic properties in the time and

frequency domains of a soft layer bonded to a rigid substrate. *Acta Biomater* 2009; 5(1): 240–248.

47. Hayes WC, Keer LM, Herrmann G, et al. A mathematical analysis for indentation tests of articular cartilage. *J Biomech* 1972; 5(5): 541–551.

48. Raub CB, Putnam AJ, Tromberg BJ, et al. Predicting bulk mechanical properties of cellularized collagen gels using multiphoton microscopy. *Acta Biomater* 2010; 6(12): 4657–4665.

49. Holdsworth A, Bradley K, Birch S, et al. Elastography of the normal canine liver, spleen and kidneys. *Vet Radiol Ultrasound* 2014; 55(6): 620–627.

50. Yamanaka N, Kaminuma C, Taketomi-Takahashi A, et al. Reliable measurement by virtual touch tissue quantification with acoustic radiation force impulse imaging: phantom study. *J Ultrasound Med* 2012; 31(8): 1239–1244.

51. Nanai B, Lyman R and Bichsel PS. Use of intraoperative ultrasonography in canine spinal cord lesions. *Vet Radiol Ultrasound* 2007; 48(3): 254–261.

52. Uri M. Density and mass of each organ/tissue – Human Homo sapiens (BNID 110245). *Bionumbers*, http://bionumbers.hms.harvard.edu/bionumber.aspx?id=110245 (accessed 1 October 2018).

53. RStudio. RStudio: integrated development environment for R, 2012, http://www.rstudio.org

54. Olby N. The pathogenesis and treatment of acute spinal cord injuries in dogs. *Vet Clin North Am Small Anim Pract* 2010; 40(5): 791–807.

55. Shin HJ, Kim M-J, Kim HY, et al. Comparison of shear wave velocities on ultrasound elastography between different machines, transducers, and acquisition depths: a phantom study. *Eur Radiol* 2016; 26(10): 3361–3367.

56. Chang S, Kim M-J, Kim J, et al. Variability of shear wave velocity using different frequencies in acoustic radiation force impulse (ARFI) elastography: a phantom and normal liver study. *Ultraschall Med* 2013; 34(3): 260–265.

57. Saxena T, Gilbert J, Stelzner D, et al. Mechanical characterization of the injured spinal cord after lateral spinal hemisection injury in the rat. *J Neurotrauma* 2012; 29: 1747–1757.

58. Mazuchowski EL and Thibauld LE. Biomechanical properties of the human spinal cord and pia mater. In: *Proceedings of the 2003 summer bioengineering conference*, Key Biscayne, FL, 25–29 June 2003, pp. 25–29, http://www.tulane.edu/~sbc2003/pdfdocs/1205.PDF

59. McKee CT, Last JA, Russell P, et al. Indentation versus tensile measurements of young's modulus for soft biological tissues. *Tissue Eng Part B Rev* 2011; 17(3): 155–164.

60. Karpushkin E, Dušková-Smrčková M, Šlouf M, et al. Rheology and porosity control of poly(2-hydroxyethyl methacrylate) hydrogels. *Polymer* 2013; 54: 661–672.

61. Oakland RJ, Hall RM, Wilcox RK, et al. The biomechanical response of spinal cord tissue to uniaxial loading. *Proc Inst Mech Eng H* 2006; 220(4): 489–492.

62. Bilston LE and Thibault LE. The mechanical properties of the human cervical spinal cord in vitro. *Ann Biomed Eng* 1996; 24(1): 67–74.

63. Bartlett RD, Choi D and Phillips JB. Biomechanical properties of the spinal cord: implications for tissue engineering and clinical translation. *Regen Med* 2016; 11(7): 659–673.

64. Ichihara K, Taguchi T, Shimada Y, et al. Gray matter of the bovine cervical spinal cord is mechanically more rigid and fragile than the white matter. *J Neurotrauma* 2001; 18(3): 361–367.

65. Cheng S, Clarke EC and Bilston LE. Rheological properties of the tissues of the central nervous system: a review. *Med Eng Phys* 2008; 30(10): 1318–1337.

66. Ramo NL, Shetye SS, Streijger F, et al. Comparison of in vivo and ex vivo viscoelastic behavior of the spinal cord. *Acta Biomater* 2018; 68: 78–89.

67. Novikova LN, Mosahebi A, Wiberg M, et al. Alginate hydrogel and matrigel as potential cell carriers for neurotransplantation. *J Biomed Mater Res A* 2006; 77(2): 242–252.

68. Wang C, Sun C, Hu Z, et al. Improved neural regeneration with olfactory ensheathing cell inoculated PLGA scaffolds in spinal cord injury adult rats. *Neurosignals* 2017; 25(1): 1–14.

69. Joosten EAJ, Bär PR and Gispen WH. Collagen implants and cortico-spinal axonal growth after mid-thoracic spinal cord lesion in the adult rat. *J Neurosci Res* 1995; 41: 481–490.

70. Li X, Xiao Z, Han J, et al. Promotion of neuronal differentiation of neural progenitor cells by using EGFR antibody functionalized collagen scaffolds for spinal cord injury repair. *Biomaterials* 2013; 34(21): 5107–5116.

71. Geissler SA, Sabin AL, Besser RR, et al. Biomimetic hydrogels direct spinal progenitor cell differentiation and promote functional recovery after spinal cord injury. *J Neural Eng* 2018; 15(2): 025004.

72. Straley KS, Foo CWP and Heilshorn SC. Biomaterial design strategies for the treatment of spinal cord injuries. *J Neurotrauma* 2010; 27(1): 1–19.

73. Epstein N. A review article on the diagnosis and treatment of cerebrospinal fluid fistulas and dural tears occurring during spinal surgery. *Surg Neurol Int* 2013; 4: S301–S317.

74. Pelham RJ and Wang Y. Cell locomotion and focal adhesions are regulated by substrate flexibility. *Proc Natl Acad Sci USA* 1997; 94: 13661–13665.

75. Discher DE, Janmey P and Wang Y-L. Tissue cells feel and respond to the stiffness of their substrate. *Science* 2005; 310: 1139–1143.

76. Guilak F, Cohen DM, Estes BT, et al. Control of stem cell fate by physical interactions with the extracellular matrix. *Cell Stem Cell* 2009; 5: 17–26.

77. Nemir S and West JL. Synthetic materials in the study of cell response to substrate rigidity. *Ann Biomed Eng* 2010; 38(1): 2–20.

78. Zhu Y, Dong Z, Wejinya UC, et al. Determination of mechanical properties of soft tissue scaffolds by atomic force microscopy nanoindentation. *J Biomech* 2011; 44: 2356–2361.

79. Ahearne M, Wilson SL, Liu K-K, et al. Influence of cell and collagen concentration on the cell–matrix mechanical relationship in a corneal stroma wound healing model. *Exp Eye Res* 2010; 91(5): 584–591.

80. Sakai S, Masuhara H, Yamada Y, et al. Transition of mechanical property of porous alginate scaffold with cells during culture period. *J Biosci Bioeng* 2005; 100(1): 127–129.

81. Khaw P, Occleston N, Schultz G, et al. Activation and suppression of fibroblast function. *Eye* 1994; 8: 188–195.

82. Moeendarbary E, Weber IP, Sheridan GK, et al. The soft mechanical signature of glial scars in the central nervous system. *Nat Commun* 2017; 8: 14787.

83. Balgude AP, Yu X, Szymanski A, et al. Agarose gel stiffness determines rate of DRG neurite extension in 3D cultures. *Biomaterials* 2001; 22(10): 1077–1084.

84. Flanagan LA, Ju Y-E, Marg B, et al. Neurite branching on deformable substrates. *Neuroreport* 2002; 13: 2411–2415.

85. Yu X and Bellamkonda RV. Dorsal root ganglia neurite extension is inhibited by mechanical and chondroitin sulfate-rich interfaces. *J Neurosci Res* 2001; 66: 303–310.

86. Franze K, Janmey PA and Guck J. Mechanics in neuronal development and repair. *Annu Rev Biomed Eng* 2013; 15: 227–251.

87. Gangatharan G, Schneider-Maunoury S and Breau MA. Role of mechanical cues in shaping neuronal morphology and connectivity. *Biol Cell* 2018; 110(6): 125–136.

88. Alaqeel A, Abou Al-Shaar H, Alaqeel A, et al. The utility of ultrasound for surgical spinal decompression. *Med Ultrason* 2015; 17(2): 211–218.

89. Anderson KD, Guest J, Dietrich WD, et al. Safety of autologous human Schwann cell transplantation in subacute thoracic spinal cord injury. *J Neurotrauma* 2017; 34: 2950–2963.